Silicon oxycarbide/nano-silicon composite anodes for Li-ion batteries: Considerable influence of nano-crystalline vs. nano-amorphous silicon embedment on the electrochemical properties

Jan Kaspar [a,*], Magdalena Graczyk-Zajac [a], Stefan Lauterbach [b], Hans-Joachim Kleebe [b], Ralf Riedel [a]

[a] Institut für Materialwissenschaft, Technische Universität Darmstadt, Disperse Feststoffe, Jovanka-Bontschits-Straße 2, 64287 Darmstadt, Germany
[b] Institut für Angewandte Geowissenschaften, Technische Universität Darmstadt, Schnittspahnstraße 9, 64287 Darmstadt, Germany

HIGHLIGHTS

- Silicon oxycarbide/nano-silicon composites as new anode material for LIB.
- Polymer-derived SiOC ceramic matrix stabilizes nano-silicon upon cycling.
- Silicon embedment enhances the intrinsic gravimetric capacity of SiOC.
- Stable reversible capacity of 704 mAh g^{-1} for nano-amorphous Si embedment.

ARTICLE INFO

ABSTRACT

Silicon oxycarbide/nano-silicon composites (SiOC/nSi) are prepared by mixing of nano-sized silicon, either crystalline (nSi_c) or amorphous (nSi_a), with commercially available polyorganosiloxane *RD-684a* and subsequent pyrolysis. The influence of the type of nano-silicon, namely crystalline vs. amorphous, on the electrochemical properties and performance is analyzed and correlated with the corresponding composite microstructure. In the case of crystalline nano-silicon, a high reversible capacity of 905 mAh g^{-1} is registered, whereas that for amorphous nano-silicon embedment reaches 704 mAh g^{-1}. However, regarding the cycling stability, SiOC/nSi_c shows a significant capacity fading upon continuous cycling, related to SiOC matrix failure. The host phase is not able to accommodate the arising mechanical stresses upon Si grain expansion and contraction when alloying/dealloying with Li. SiOC/nSi_a on the contrary, demonstrates a stable cycling performance for up to 100 cycles. This excellent performance is explained by the enhanced matrix integrity of the compound, rationalized by a smaller size of the embedded crystallized Si grains and an intrinsically enhanced electrical conductivity due to the formation of SiC.

1. Introduction

Li-ion batteries are well commercialized and widely used as energy source for all kind of portable electronics. However, there is an unsatisfied need for higher energy and power density devices, for instance, as power sources for electrically driven cars or large scale stationary energy storage [1–3]. Hence, novel electrode and electrolyte materials are required in order to provide a prospective future for Li-ion battery technology; in particular, alternatives to graphite with its limited capacity of 372 mAh g^{-1} need to be found [4–6].

One alternative compound attracting much attention in the last years is silicon, due to its high electrochemical capacity of 3579 mAh g^{-1} for Li$_{15}$Si$_4$ phase. Unfortunately, Si suffers from large volume changes upon alloying with Li ($\Delta V \approx 280\%$ for Si/Li$_{15}$Si$_4$), creating strong mechanical stresses, which cause particles to crack and pulverize. In consequence, electrical conduction pathways break down, leading to electrode failure and poor cycle life-time [7–13]. To overcome these drawbacks research efforts have been in progress in order to improve the stability of silicon based anodes.

* Corresponding author. Tel.: +49 6151 16 6343; fax: +49 6151 16 6346.
E-mail address: kaspar@materials.tu-darmstadt.de (J. Kaspar).

The size reduction to the nano-metric scale is intensively explored to overcome the electrode failure [11,14–18]. Various studies have shown a considerable increase in the reversible capacity and life-time for silicon thin-films [19,20], silicon nano-wires [21–27] and silicon nano-tubes [28,29]. Another promising and efficient approach represents the embedding of silicon within active and non-active matrices, leading to the diminution of the overall capacity but increasing the cycling stability of the composite material. The huge number of scientific report related to this matter has been reviewed by Kasavajjula et al. [30]. Within this context, the preparation of Si-carbon-composites or the selective carbon-coating of silicon has to be mentioned as a particularly successful way to stabilize silicon [31–44].

Besides silicon, polymer-derived ceramics (PDC), that provide a high amount of free carbon within their microstructure, are considered as highly promising anode compounds (SiOC: [45–62], SiCN: [63–66]). In addition to PDC preparation, SiOC can be produced by Sol–Gel process [67–71] or via electrodeposition method [72–74]. Since the early work of Dahn et al. [75–80], continuous research was done in order to introduce SiOC based anodes to commercial Li-ion cells. First investigations on SiOC–CNT composites were addressed by Shen et al. and Bhandavat et al. [81–83] and the synthesis and electrochemical properties of Sol–Gel derived Si/SiOC composites reported by Liu et al. [84]. The modeling of carbon-rich SiOC and its Li-insertion was accomplished by P. Kroll [85–88]. However, for practical application of SiOC anodes, the decrease of the first cycle irreversible capacity still represents a major challenge for this material. In general the charge storage capacity of SiOC ceramics is closely related to their microstructure and phase composition, which can be systematically designed and tailored in the PDC process by selecting suitable precursors, their chemical modification and variation of processing conditions. Concerning the microstructure of carbon-rich SiOC (i.e. compounds in which the content of carbon exceeds 20 wt-% [89]), it is composed of two interpenetrating phases: i) an amorphous silica and/or Si–O–C network comprised of $SiO_{4−x}C_x$ ($x = 1–4$) structural units and ii) a free carbon phase comprised of amorphous or turbostratic-like carbon [90–94]. Depending on the amount of carbon segregation, either carbon nano-domains (low amount of free C) or a carbon percolation network (high amount of free C) exist, as demonstrated by electrical conductivity measurements and TEM analysis [95–97].

Lithium-ion storage in carbon-rich SiOC occurs in form of an adsorption and surface storage within the free carbon phase, similar to the storage of Li-ions in disordered carbons; host sites are the edges of graphene sheets, interstitial and defect sites, micropores and graphite nano-crystallites. On the contrary, the Si–O–C amorphous network is attributed a minor role in the reversible storage process [45,51–53,58–60]. In addition, the storage of lithium ions within the phase-boundary of the Si–O–C network and free carbon phase, described by the nano-domain model, is discussed in the literature as well [81,98–101]. Due to the high amount of free carbon interspersed within the amorphous Si–O–C network, carbon-rich silicon oxycarbide represents a promising electrochemically active matrix to stabilize silicon with respect to continuous lithiation/delithiation. In contrast to graphite, carbon-rich SiOC provides a higher Li-ion storage capacity as host, namely up to 520 mAh g^{-1} [59] instead of only 372 mAh g^{-1}, as known for graphite.

In this paper, we report for the first time, that the combination of nano-scaled silicon and carbon-rich SiOC brings about a promising electrochemical performance of the final composite. In particular it makes possible to i) take advantage of the specific electrochemical properties of both compounds, ii) profit of the elastic properties of SiOC to accommodate the volume changes related to Li–Si alloy formation and thus enhance the materials cycle-ability and iii) ensure a sufficient intrinsically electrical conductivity thanks to the high carbon content in the SiOC ceramic. Moreover, we investigate the role of the embedded silicon crystallinity on the composite electrochemical stability. Thus, crystalline and amorphous silicon particles were mixed with commercially available polyorganosiloxane *RD-684a* and subsequently thermally treated at 1100 °C for SiOC matrix ceramization. The influence of the silicon crystallinity on the microstructure of the composites is analyzed, compared and discussed with respect to the corresponding electrochemical properties and cycling behavior. Surprisingly, the microstructure significantly depends on the embedded silicon, i.e. amorphous Si crystallizes and reacts with free carbon under pyrolysis condition and strong SiC crystallization occurs, while for the composite prepared with crystalline silicon, Si grains of larger diameter and only traces of crystalline SiC are found, as verified by XRD and TEM analysis.

2. Experimental

Silicon oxycarbide/nano-silicon composites (SiOC/nSi) were prepared by mixing of nano-crystalline (nSi_c, 30–50 nm; Nano-structured & Amorphous Materials Inc., USA) and nano-amorphous (nSi_a, ~36 nm; Strem Chemicals Inc., Germany) silicon particles with polyorganosiloxane *RD-684a* (Starfire Systems Inc., USA) in acetone. The amount of solvent was adjusted to the double amount of polymer by weight and removed before pyrolysis by vacuum drying. The mixing itself was accomplished by magnetic stirring with ultrasonic support. Pyrolysis of the mixed batches was performed under Ar-atmosphere at a temperature of 1100 °C using quartz-equipment; holding time at the maximum temperature was 3 h and heating rates set to 100 °C h^{-1}. The amount of Si to polymer of the prepared mixtures was adjusted to generate composites with a weight-ratio of Si:SiOC phase of about 20:80, as suggested beneficial for silicon-based composites for anode purposes [102].

For microstructural characterization, X-ray powder diffraction (XRD) was performed with a Bruker D8 Advance (Bruker, USA), using Ni-filtered Cu Kα radiation. For elemental analysis, a carbon analyzer Leco-200 (Leco Corporation, USA) was used to determine the carbon content and an N/O analyzer Leco TC-436 (Leco Corporation, USA) to determine the corresponding oxygen content. The silicon fraction was calculated as the difference to 100 wt-% of the sum of the wt-% values of carbon and oxygen, assuming no other elements being present in the samples. Raman spectra were recorded with a confocal micro-Raman spectrometer Horiba HR 800 (Horiba, Japan), using an Ar-ion laser with wavelength 514.5 nm. Scanning electron microscopy (SEM) images of uncycled and cycled electrodes were recorded with a Philips XL30 FEG (FEI, Netherlands). Transmission electron microscopy (TEM) studies on powder samples dispersed on a lacey carbon Cu-grid were performed at a JEOL 2100F instrument (JEOL, Japan), operated at 200 keV.

For electrochemical measurements, electrodes composed of 85 wt-% composite material (active mass), 5 wt-% Carbon black (Timcal Ltd., Switzerland) and 10 wt-% Na-CMC binder (Sigma-–Aldrich, USA), were prepared by tape-casting. The film thickness after drying of the tapes was around ~36 μm in average, with a loading of the active material of about 1.4 mg cm^{-2}. A detailed procedure of electrode preparation can be found elsewhere [53,59]. Testing-cells of two-electrode Swagelok-type were assembled in an Ar-filled glove-box, using metallic lithium (Li-tape 99.9% purity, 0.75 mm thickness, Alfa Aesar, UK) as reference/counter electrode, 1 M LiPF$_6$ in EC:DMC ratio 1:1 (LP30, Merck KGaA, Germany) as electrolyte and glass fiber filter (Whatman™, UK) as separator. Hermetically closed cells were cycled with a VMP multipotentiostat
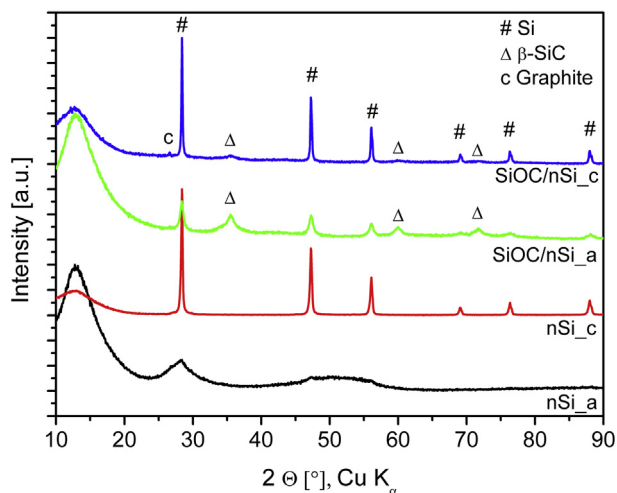
Fig. 1. XRD pattern of SiOC/nSi_c and SiOC/nSi_a composites and pure input silicon nSi_c and nSi_a.
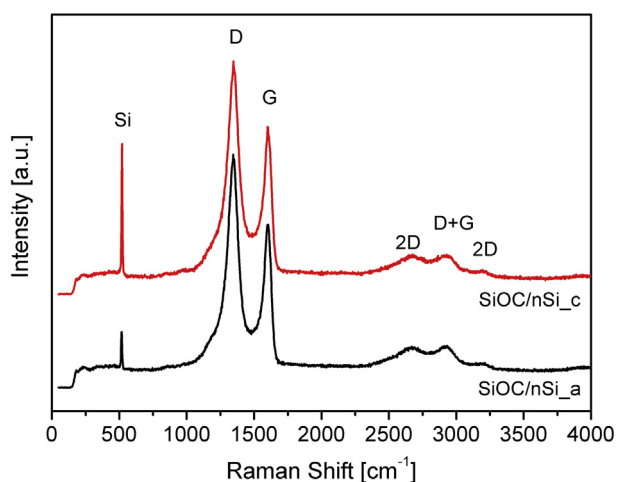

Fig. 2. Raman spectra of SiOC/nSi_c and SiOC/nSi_a composites.

(BioLogic Science Instruments, France) by galvanostatic cycling with potential limitation (GCPL) at a current rate of 74 mA g^{-1} within the potential range of 0.005–3 V (E vs. Li/Li$^+$) and potentiodynamic cycling with galvanostatic acceleration (PCGA) in 50 mV steps with a limiting current of 37 mA g^{-1} and within the potential window of 0.05–3 V (E vs. Li/Li$^+$). For data analysis, the registered capacities were divided by the mass of active material, i.e. the sum of the masses of SiOC and nSi phase.

In the following, composites and electrodes are denoted with respect to the morphology of the initial embedded silicon

particles, i.e. SiOC/nSi_c for crystalline and SiOC/nSi_a for amorphous species.

3. Results and discussion

3.1. Material characterization

Fig. 1 presents the X-ray diffraction pattern for the SiOC/nSi_c and SiOC/nSi_a composites, as well as diffractograms of the initially used silicon powders nSi_c and nSi_a. In both composite patterns and for nSi_c, strong Bragg reflections related to crystalline silicon are visible at 28.4°, 47.3°, 56.1°, 69.1°, 76.4° and 88.0° (reference card number [27-1402]). Crystalline silicon carbide (β-SiC) can be identified for the composites at 35.6°, 60.0° and 71.8° (reference card number [29-1129]). For SiOC/nSi_c there is an additional weak reflex visible at 26.5° originating from diffraction at graphitic carbon arrangements within the free carbon phase in the SiOC matrix [53,59]. The pattern of nSi_a reveals the amorphous nature of the material, since no sharp reflexes are observed, but rather broad signals around 28° and in the range of 47–55°. The presence of crystalline silicon in SiOC/nSi_a indicates that the initially amorphous Si crystallizes under pyrolysis conditions, at least partially. A similar behavior was reported for the thermal treatment of pure amorphous nano-silicon by Schierning et al. [103]. The intensity of the SiC signals is much stronger in case of SiOC/nSi_a, suggesting a strong carbothermal reaction of the amorphous silicon with free carbon present in the SiOC matrix. SiC crystallization by decomposition of the matrix itself can be excluded, since pure SiOC derived from *RD-684a* polymer is exclusively amorphous up to 1200 °C [53,59]. In contrast, for SiOC/nSi_c only week SiC intensities are detected, suggesting the formation of minor amounts of SiC. A Riedvelt refinement was applied for the SiOC/nSi_a pattern in order to analyze the phase ratio between the crystallized silicon and silicon carbide. The results indicate a ratio of Si:SiC of 28.5:71.5 by weight and 36.3:63.7 by mole.

The existence of segregated free carbon is outlined by the presence of intense D and G-bands in the Raman spectra of the composites, as shown in Fig. 2. Besides the D and G-intensities, the overtones of the D vibration, the 2D modes, the D + G combination mode and a sharp band relating to crystalline Si-vibration are visible. In particular, the intense D-band specifies the free carbon of amorphous nature, well corresponding to the absence of graphite diffraction intensity in the XRD patterns.

Table 1 presents the chemical composition of the composites and their ceramic matrices. For all species a phase partitioning of SiOC into equivalents of silicon carbide, silica and free carbon is included, according to [71]. For the composites, the phase fractions of crystalline Si and SiC are additionally quantified. In the case of SiOC/nSi_a, the estimated ratio Si:SiC (28.5:71.5 by weight and 36.3:63.7 by mole) is taken as the basis for Si and SiC quantification, assuming the consumption of free carbon from the matrix in the

Table 1
Chemical composition of SiOC/nSi_c and SiOC/nSi_a. The weight fractions of the phase equivalents for SiOC, i.e. silicon carbide, silica and free carbon, are quantified according to Ref. [71].

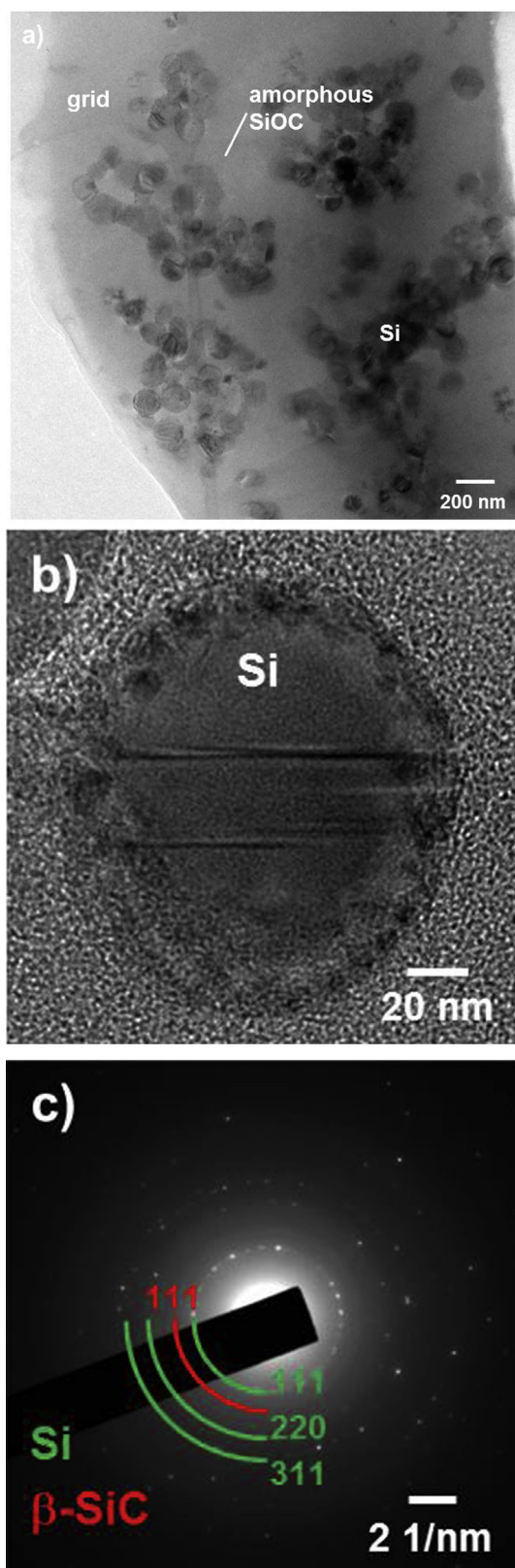| Sample	Si [wt-%]	O [wt-%]	C [wt-%]	Phase equivalents SiOC			Crystalline Si [wt-%]	Crystalline SiC [wt-%]
				SiC [wt-%]	SiO$_2$ [wt-%]	Free C [wt-%]		
SiOC/nSi_c	43.68	15.25	41.07	14.70	28.63	36.67	20.00	–
SiOC/nSi_c matrix only	29.60	19.06	51.34	18.37	35.79	45.83	–	–
SiOC/nSi_a	42.67	16.15	41.18	12.13	30.32	32.10	7.25	18.20
SiOC/nSi_a matrix only	30.41	21.66	47.93	16.27	40.68	43.05	–	–

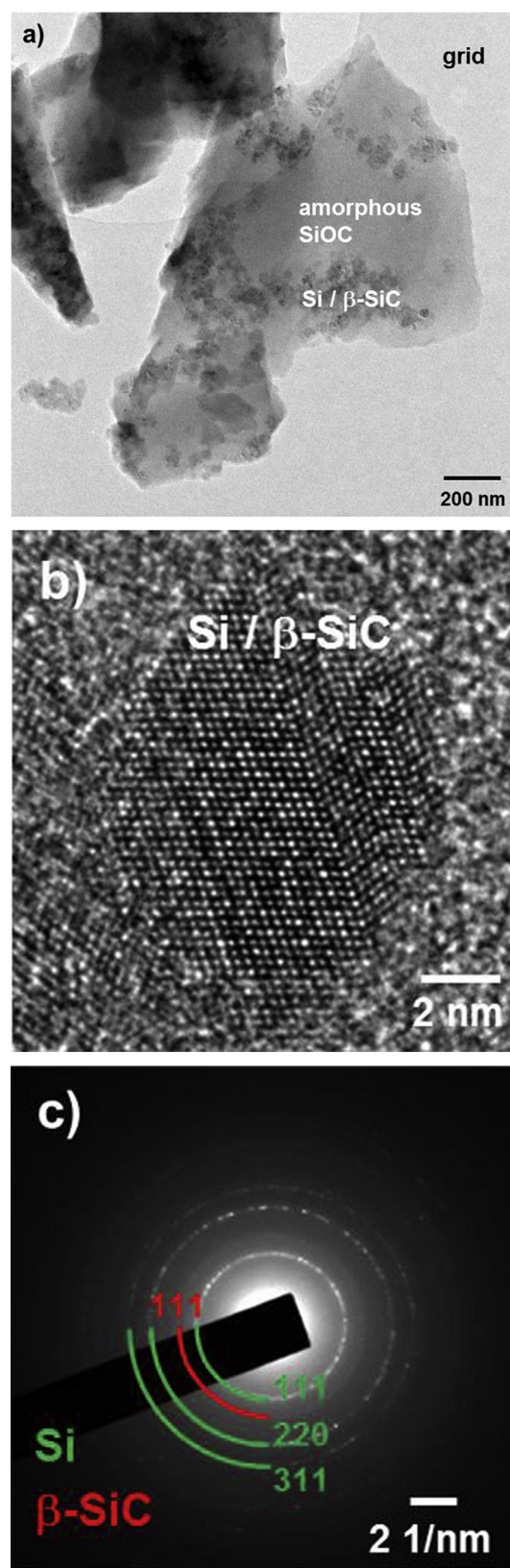**Fig. 3.** a), b) TEM micrographs and c) SAED pattern of SiOC/nSi_c.

Fig. 4. a), b) TEM micrographs and c) SAED pattern of SiOC/nSi_a; in HRTEM in the present orientation there is no identification between Si and SiC possible.

formation process of SiC. Consequently, the actual amount of crystalline Si phase in SiOC/nSi_a only amounts 7.25 wt-% in contrast to 20 wt-% present in SiOC/nSi_c.

In Figs. 3 and 4, the TEM micrographs and the SAED pattern of SiOC/nSi_c and SiOC/nSi_a are shown. Note that for both composites, the particle distribution within the matrix is inhomogeneous, as a result of sample preparation, since the nano-sized silicon particles already tend to agglomerate before mixing with poly-organosiloxane *RD-684a*. In the case of SiOC/nSi_c, grains of the initially embedded size of 30−50 nm and particles up to 100 nm in diameter are well visible within the amorphous SiOC phase. In contrast, the microstructure of SiOC/nSi_a differs significantly, i.e. Si and SiC precipitates of ~10 nm in size are detected. Due to the similar lattice parameter of Si and β-SiC, HRTEM is not able to distinguish between both species. However, the SAED pattern clearly reveals the presence of both phases, well matching with the XRD results.

Altogether, the prepared SiOC/nSi composites are composed of four major phases: i) the amorphous Si−O−C matrix, including ii) free carbon, iii) crystalline silicon and iv) crystalline silicon carbide.

3.2. Electrochemical characterization

The electrochemical stability of both composites, SiOC/nSi_c and SiOC/nSi_a, upon prolonged galvanostatic cycling performed with a current of 74 mA g^{-1} is compared in Fig. 5. For SiOC/nSi_c, the initial reversible capacity amounts 804 mAh g^{-1} and increases during the first 10 cycles up to 905 mAh g^{-1}. Starting around cycle 15, a continuous capacity decrease sets on and after 50 cycles a capacity of only 314 mAh g^{-1} is recovered. The coulombic efficiency within one cycle ranges between 94 and 98%. It is suggested that the reason of the observed fading is related to the loss of silicon electroactivity, due to a progressive degradation and failure of the SiOC matrix, which is not able to withstand the generated mechanical stresses upon continuous expansion and contraction during Li−Si alloying/dealloying. At a certain point, the matrix ruptures irreversibly, leading to electrically isolated fragments that cannot contribute to Li-ion storage any-longer. For SiOC/nSi_a, the initial capacity is lower compared to that of SiOC/nSi_c (Fig. 5), due to the loss of electrochemically active silicon and free carbon by the formation of inactive silicon carbide [104]. The initial recovered capacity of 555 mAh g^{-1} increases up to a maximum of 704 mAh g^{-1} and remains relatively stable for 100 cycles. Characteristic fading, as observed for SiOC/nSi_c, does not occur, demonstrating superior
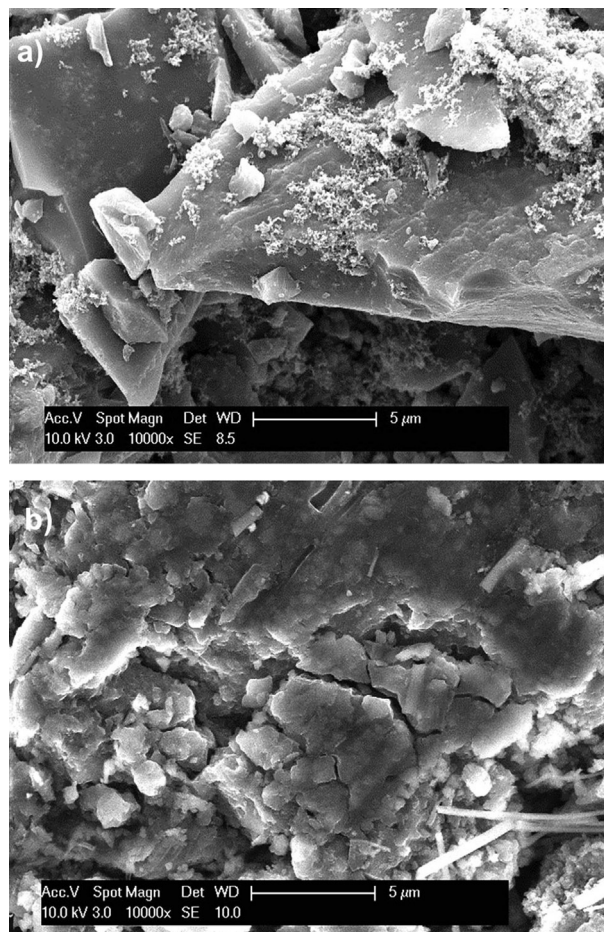

Fig. 6. SEM images of SiOC/nSi_c electrodes a) before and b) after cycling; the fibers present remaining rests of the separator.

matrix integrity of the sample. Moreover, the coulombic efficiency after the 5th cycle is continuously above 99.5%.

SEM micrographs of uncycled and cycled composite electrodes are shown in Figs. 6 and 7 and illustrate the matrix failure of SiOC/nSi_c and matrix integrity of SiOC/nSi_a. The prolonged insertion/extraction of lithium into SiOC/nSi_c causes significant cracking of the electrode particles and in consequence, the composite grains appear broken apart and pulverized after cycling. For SiOC/nSi_a on the contrary, almost no change in morphology is found, when comparing the pristine electrode to that exposed to prolonged electrochemical cycling.

The differential capacity plots for both composites are shown in Fig. 8 and confirm the prior findings. When following the development of the Li−Si alloying/dealloying activity, at 0.22 and 0.08 V for alloying and at 0.30 and 0.45 V for dealloying [10], an initial intensity increase is recognized for SiOC/nSi_c, followed by a rapid decrease after cycle 10 (Fig. 8a). The initial capacity increase relates to cycle-wise silicon activation, suggesting that not all silicon present in the sample is contributing to Li-ion storage right from the beginning of cycling and that the Si phase needs to be activated first. The general intensity decrease in the dq/dV plot over the whole potential range beyond cycle 10, again is attributed to the continuous degradation of the composite material due to matrix failure and matches well with the cycling performance shown in Fig. 5. For SiOC/nSi_a on the contrary (Fig. 8b), the characteristic Li−Si alloying/dealloying signals initially increase in intensity
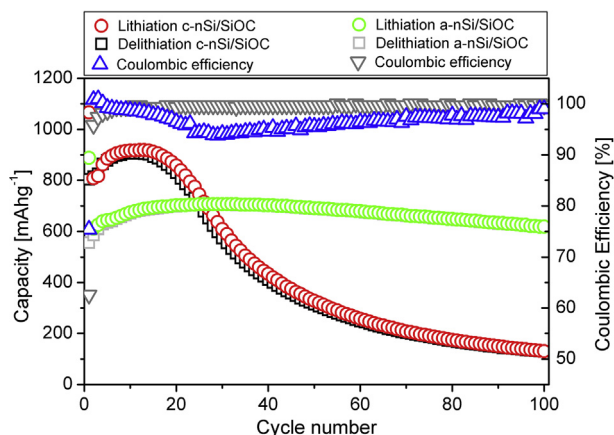

Fig. 5. Comparison of the cycling behavior and coulombic efficiency of SiOC/nSi_c and SiOC/nSi_a in dependence of cycle number at a current rate of 74 mA g^{-1}.
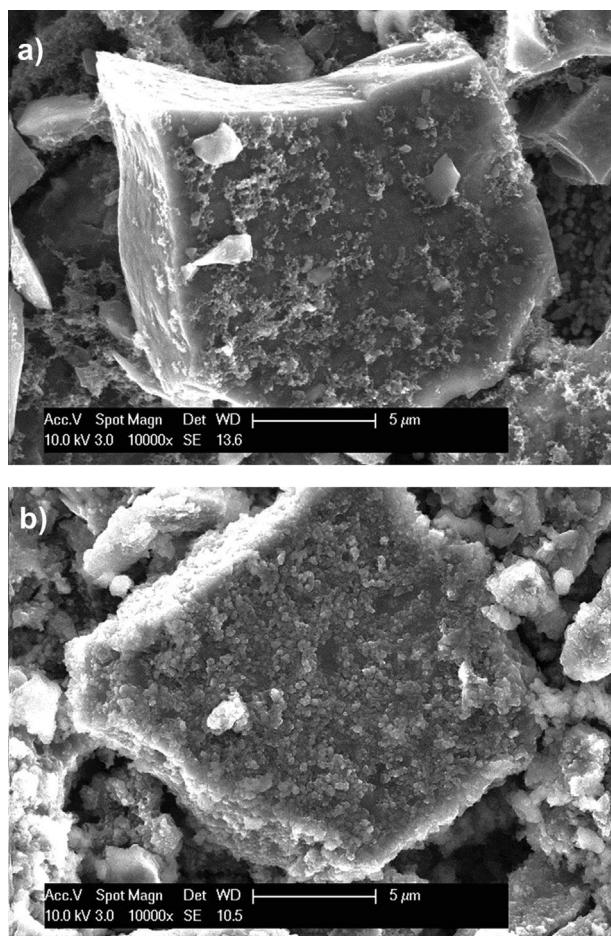
Fig. 7. SEM images of SiOC/nSi_a electrodes a) before and b) after cycling.

Fig. 8. Differential capacity curves for a) SiOC/nSi_c and b) SiOC/nSi_a.

within the first 10 cycles and remain stable in following prolonged cycling.

Note that in both plots, there is a difference in the first alloying curve in the cathodic branch, namely for SiOC/nSi_c (Fig. 8a) a peak at ~0.18 V, followed by an intense peak in the range of 0.12−0 V, is visible, while for SiOC/nSi_a (Fig. 8b) a broad wave starting at ~0.22 V, superimposing with a potential peak at ~0.18 V and again followed by a low voltage peak in the range of 0.12−0 V, is identified. The peak at 0.18 V can be attributed to the activity of the SiOC matrix, observed at this potential during the first lithiation [105]. The low voltage peak in the range of 0.12−0.08 V for both samples corresponds to the first alloying of crystalline silicon and the formation of a two-phase region with a-Li$_x$Si, as described by Obrovac et al. [9] and Li et al. [10] (Si_c + xLi → a-Li$_x$Si). For SiOC/nSi_a first the activity of the traces of amorphous silicon present in the composite at ~0.22 V is observed, but superimposed within the more pronounced SiOC matrix electroactivity appearing at potentials around 0.18 V.

Within subsequent cycling both composites reveal the high and low voltage peaks of amorphous silicon at ~0.22 and 0.08 V in the cathodic branch [10], while the matrix electroactivity at 0.18 V is replaced by a broad peak with maximum at ~0.45 V [60,105]. This activity remains stable for SiOC/nSi_a, while it almost vanishes for SiOC/nSi_c after cycle 40 (Fig. 8a, yellow curve (in the web version)). This finding matches perfectly to our reasoning that the electrochemical instability of the SiOC/nSi_c composite is caused by the inability of the matrix to withstand the stresses related to the
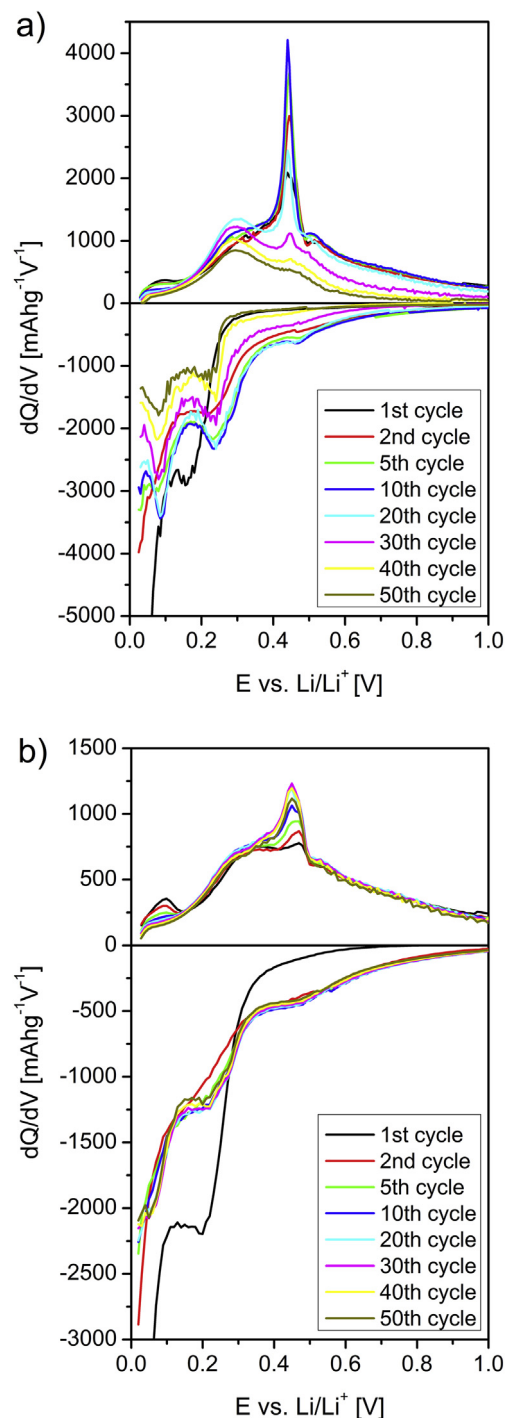
silicon volume changes. Concerning the SiOC activity in the anodic branch, typically peaks are found at potentials of 0.08, 0.34 and 0.68 V [60]. For both composites, not all these signals are well pronounced, but rather broadened and overlapping with the silicon activity intensities. It is however possible to trace the significant fading of the 0.08 and 0.68 V peaks for SiOC/nSi_c with subsequent cycling, emphasizing the diminishing matrix activity.

In Fig. 9, the cycling performance of the composites is compared with respect to pure SiOC and a pure nSi_c reference, representing the general cycling behavior of both, pure nSi_c and nSi_a reference
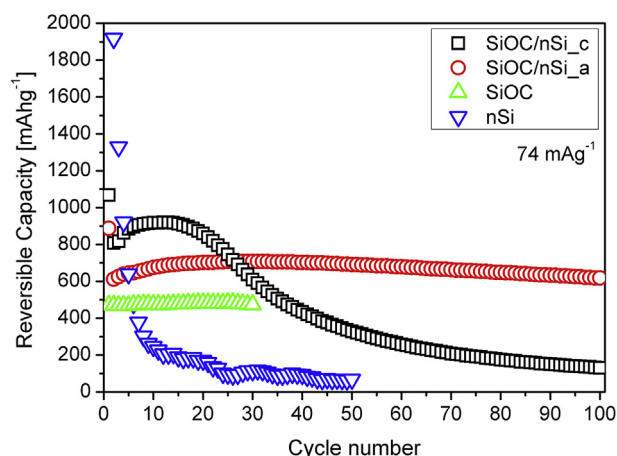
Fig. 9. Comparison of the reversible capacity in dependence of cycle number for SiOC/nSi_c, SiOC/nSi_a, pure SiOC [53,59] and pure nSi at a cycling current of 74 mA g^{-1}.

electrodes. The data for pure SiOC is taken form our previous reports [53,59]. The capacity of the nSi electrode drops instantly and after 10 cycles only about 10% of the initial capacity is recovered. This rapid degradation is a well-known and reported phenomenon, rationalized by the tremendous volume changes upon Li–Si alloying/dealloying (Si/Li$_{15}$Si$_4$, $\Delta V \approx 280\%$) that provokes amorphization and pulverization of the electrode [7–13]. Pure SiOC demonstrates a stable capacity of about 477 mAh g^{-1}. For both SiOC/nSi composites, the introduction of electrochemically active silicon increases the total capacity up to 905 mAh g^{-1} for SiOC/nSi_c and 704 mAh g^{-1} for SiOC/nSi_a compared to pure SiOC. However, in the case of crystalline silicon embedment, the cycling stability and electrode life-time are significantly reduced. Moreover, with respect to pure silicon, a carbon-rich SiOC host appears suitable to mechanically stabilize the incorporated Si-grains during lithium uptake and release and accounts for an improved cycling stability and reduced capacity fading, especially in the case of SiOC/nSi_a. When comparing the absolute capacities of both composites to the ones reported for Si/Graphite composites by Jo et al. [41], a carbon-rich SiOC matrix offers additional advantage, since the theoretical capacity of graphite is limited to 372 mAh g^{-1}, whereas SiOC exceeds this value with up to 520 mAh g^{-1} [53,59]. Accordingly, slightly lower capacity values of 530 and 568 mAh g^{-1} were registered for the Si/Graphite samples of similar composition of Si:Graphite of 20:80 by weight. Another report in literature is concerned with the electrochemical performance of a Si/SiOC composite prepared by Sol–Gel method [84]. The ratio of Si:SiOC amounts approximately 10:90 by weight, whereas the sample demonstrates a high first cycle reversible capacity of 1372 mAh g^{-1}. Upon prolonged cycling the recovered capacity rapidly decreases, with only 77% capacity retention after 30 cycles (990 mAh g^{-1}). In comparison, the SiOC/nSi_a sample prepared in this work exhibits a slightly lower content of free Si (7.25 wt-%) and hence a lower maximum capacity (704 mAh g^{-1}). However, the synthesized SiOC/nSi_a composite stands out with its superior cycling stability, i.e. 88% capacity retention after 100 cycles with respect to the maximum value, indicating that a carbon-rich SiOC host can better accommodate the arising mechanical stresses upon Li–Si alloy expansion/contraction than carbon-poor SiOC, as prepared by Liu et al. [84]. A similar beneficial stabilization was recently reported for SiOC/Sn nano-composites, in which a carbon-rich SiOC matrix was emphasized of major importance for the non-destructive buffering of Sn-grain related volume changes upon alloying/dealloying with Li [106].

On the one hand, the smaller size of the crystalline nSi grains (~10 nm), causes minor absolute volume changes upon Li–Si alloying/dealloying and in consequence less mechanical load is applied to the matrix. As consequence, critical fracture stress intensities are locally avoided. In addition, the presence of SiC phase, as in the case of SiOC/nSi_a, increases the intrinsic electrical conductivity of the material and supports the internal electrical wiring ($\sigma_{SiC} = $ ~10^1–10^2 S m^{-1} depending on its form and size, $\sigma_{Si} = 10^{-3}$ S m^{-1}, $\sigma_{SiOC} = 7.14$ S m^{-1} [97,107]). A similar conductivity increase was previously reported for SiC containing SiCN ceramics [108,109]. Finally, both features account for the superior electrochemical cycling stability of the SiOC/nSi_a material.

At last, a comparison between the theoretically expectable and the experimentally registered capacities for the composites is drawn. According to the chemical composition in Table 1, a theoretical capacity can be estimated from the mass ratio SiOC:Si. For silicon, 3579 mAh g^{-1} (Li$_{15}$Si$_4$ phase) is considered as theoretical value, whereas the capacity contribution from SiOC is adopted from our previous reports [53,59], i.e. 477 mAh g^{-1} for a current rate of 74 mA g^{-1}. In sum, the calculated values for the composites amount 1097 mAh g^{-1} for SiOC/nSi_c and 615 mAh g^{-1} for SiOC/nSi_a. For SiOC/nSi_c the experimental value of 905 mAh g^{-1} is lower compared to the theoretical one, which can be reasoned by two oppositional effects: i) the silicon phase is gradually activated upon cycling and not completely accessible for Li-ions from the first lithiation, but ii) matrix degradation and thus loss of composite active material occurs immediately upon cycling. For SiOC/nSi_a on the contrary, the experimentally found capacity of 704 mAh g^{-1} is higher than the theoretically estimated one (615 mAh g^{-1}), which could be explained by the following. First, the estimation relies on the assumption that the amorphous input silicon completely crystallizes into either silicon or silicon carbide. But it seems that amorphous silicon phase is still present within the SiOC matrix, as traced in the dq/dV plot in Fig. 8b. In consequence, the real capacity is necessarily higher than the calculated one. In addition, the presence of SiC nano-particles increases the electronic conductivity and availability of carbon phase within the SiOC host and might increase the capacity of the sample in a non-linear way with respect to the calculation. A similar phenomenon was previously reported for mixtures of carbon-poor SiCN ceramics and graphite [64,105].

4. Conclusions

Nano-crystalline and nano-amorphous silicon particles were successfully embedded within a polymer-derived, carbon-rich silicon oxycarbide matrix. The composites demonstrated a high gravimetric capacity of 905 mAh g^{-1} and 704 mAh g^{-1} for SiOC/nSi_c and SiOC/nSi_a, respectively. However, strong capacity fading was found for the SiOC/nSi_c material, whereas the incorporation of nano-amorphous Si into the SiOC matrix provided a material with a stable cycling performance up to 100 cycles. Fundamental microstructural differences were identified as the main reason for the difference in the electrochemical behavior. In the case of SiOC/nSi_c, crystalline silicon grains up to 100 nm in diameter are present within the matrix, while in the case of SiOC/nSi_a, silicon and silicon carbide crystallites of ~10 nm in size were found. Due to the smaller size of the Si precipitates, the absolute volume expansion of the formed Li–Si alloy in SiOC/nSi_a is less critical, leading to minor mechanical load locally applied to the matrix. The arising stresses can be well accommodated by the SiOC host without degradation. In the case of SiOC/nSi_c, the expansion of the larger Si grains causes a severe matrix failure and in consequence fading of the capacity is well pronounced. Moreover, nano-sized SiC grains present in SiOC/nSi_a, increase the electrical conductivity and

contribute to the superior electrochemical behavior of the composite. Finally, the deviation between the theoretically estimated capacity of SiOC/nSi_a (651 mAh g^{-1}) and SiOC/nSi_c (1097 mAh g^{-1}) and the registered ones of 704 mAh g^{-1} and 905 mAh g^{-1}, respectively, is described. For the sample based on amorphous silicon, it is suggested that the initially amorphous silicon crystallized only partially, leaving electrochemically active amorphous phase unconsidered in the estimation, while for SiOC/nSi_c a slow activation of the available crystalline silicon is assumed to be responsible for registered lower capacity values.

Acknowledgments

References

[1] H. Kawamoto, Sci. Technol. Trends 36 (2010) 34.
[2] G.L. Soloveichik, Annu. Rev. Chem. Biomol. Eng. 2 (2011) 503–527.
[3] J. Liu, Adv. Funct. Mater. 23 (2013) 924–928.
[4] C.M. Hayner, X. Zhao, H.H. Kung, Annu. Rev. Chem. Biomol. Eng. 3 (2012) 445–471.
[5] J. Chen, Materials 6 (2013) 156–183.
[6] R. Wagner, N. Preschitschek, S. Passerini, J. Leker, M. Winter, J. Appl. Electrochem. 43 (2013) 481–496.
[7] L.Y. Beaulieu, K.W. Eberman, R.L. Turner, L.J. Krause, J.R. Dahn, Electrochem. Solid-State Lett. 4 (2001) A137–A140.
[8] M.N. Obrovac, L. Christensen, Electrochem. Solid-State Lett. 7 (2004) A93–A96.
[9] M.N. Obrovac, L.J. Krause, J. Electrochem. Soc. 154 (2007) A103–A108.
[10] J. Li, J.R. Dahn, J. Electrochem. Soc. 154 (2007) A156–A161.
[11] X.H. Liu, L. Zhong, S. Huang, S.X. Mao, T. Zhu, J.Y. Huang, ACS Nano 6 (2012) 1522–1531.
[12] Y.F. Gao, M. Zhou, J. Power Sources 230 (2013) 176–193.
[13] Z. Ma, T. Li, Y.L. Huang, J. Liu, Y. Zhou, D. Xue, RSC Adv. 3 (2013) 7398–7402.
[14] J. Graetz, C.C. Ahn, R. Yazami, B. Fultz, Electrochem. Solid-State Lett. 6 (2003) A194–A197.
[15] M. Holzapfel, H. Buqa, L.J. Hardwick, M. Hahn, A. Wursig, W. Scheifele, P. Novak, R. Kotz, C. Veit, F.M. Petrat, Electrochim. Acta 52 (2006) 973–978.
[16] D. Arquier, G. Calleja, G. Cerveau, R.J.P. Corriu, C. R. Chim. 10 (2007) 795–802.
[17] J.R. Szczech, S. Jin, Energy Environ. Sci. 4 (2011) 56–72.
[18] C.-F. Sun, K. Karki, Z. Jia, H. Liao, Y. Zhang, T. Li, Y. Qi, J. Cumings, G.W. Rubloff, Y. Wang, ACS Nano 7 (2013) 2717–2724.
[19] J.P. Maranchi, A.F. Hepp, P.N. Kumta, Electrochem. Solid-State Lett. 6 (2003) A198–A201.
[20] V. Baranchugov, E. Markevich, E. Pollak, G. Salitra, D. Aurbach, Electrochem. Commun. 9 (2007) 796–800.
[21] C.K. Chan, H. Peng, G. Liu, K. Mc Ilwrath, X.F. Zhang, R.A. Huggins, Y. Cui, Nat. Nanotechnol. 3 (2008) 31–35.
[22] C.K. Chan, R. Ruffo, S.S. Hong, R.A. Huggins, Y. Cui, J. Power Sources 189 (2009) 34–39.
[23] L.-F. Cui, R. Ruffo, C.K. Chan, H. Peng, Y. Cui, Nano Lett. 9 (2009) 491–495.
[24] Y.F. Gao, M. Zhou, J. Appl. Phys. 109 (2011) 014310.
[25] A. Vlad, A.L.M. Reddy, A. Ajayan, N. Singh, J.-F. Gohy, S. Melinte, P.M. Ajayan, Proc. Natl. Acad. Sci. 109 (2012) 15168–15173.
[26] M. Ge, J. Rong, X. Fang, C. Zhou, Nano Lett. 12 (2012) 2318–2323.
[27] X.H. Liu, F. Fan, H. Yang, S. Zhang, J.Y. Huang, T. Zhu, ACS Nano 7 (2013) 1495–1503.
[28] Y. Fan, Q. Zhang, Q. Xiao, X. Wang, K. Huang, Carbon 59 (2013) 264–269.
[29] Z. Wen, G. Lu, S. Mao, H. Kim, S. Cui, K. Yu, X. Huang, P.T. Hurley, O. Mao, J. Chen, Electrochem. Commun. 29 (2013) 37–70.
[30] U. Kasavajjula, C. Wang, A.J. Appleby, J. Power Sources 163 (2007) 1003–1039.
[31] N. Dimov, S. Kugino, M. Yoshio, Electrochim. Acta 48 (2003) 1579–1587.
[32] Y. Liu, K. Hanai, J. Yang, N. Imanishi, A. Hirano, Y. Takeda, Solid State Ionics 168 (2004) 61–68.
[33] M. Holzapfel, H. Buqua, W. Scheifele, P. Novak, F.M. Petrat, Chem. Commun. 12 (2005) 1566–1568.
[34] S.H. Ng, J.Z. Wang, D. Wexler, K. Konstantinov, Z.P. Guo, H.K. Liu, Angew. Chem. Int. Ed. 45 (2006) 6896–6899.
[35] X.L. Yang, Z.Y. Wen, X.X. Xu, B. Lin, Z.X. Lin, J. Electrochem. Soc. 153 (2006) A1341–A1344.
[36] J. Saint, M. Morcrette, D. Larcher, L. Laffont, S. Beattie, J.P. Peres, D. Talaga, M. Couzi, J.M. Tarascon, Adv. Funct. Mater. 17 (2007) 1765–1774.
[37] M. Alias, O. Crosnier, I. Sandu, G. Jestin, A. Papadimopoulos, F. Le Cras, D.M. Schleich, T. Brousse, J. Power Sources 174 (2007) 900–904.
[38] R. Demir Cakan, M.-M. Titirici, M. Antonietti, G. Cui, J. Maier, Y.-S. Hu, Chem. Commun. 37 (2008) 3759–3761.
[39] C. Martin, M. Alias, F. Christien, O. Crosnier, D. Belanger, T. Brousse, Adv. Mater. 21 (2009) 4735–4741.
[40] Z. Luo, D. Fan, X. Liu, H. Mao, C. Yao, Z. Deng, J. Power Sources 189 (2009) 16–21.
[41] Y.N. Jo, Y. Kim, J.S. Kim, J.H. Song, K.J. Kim, C.Y. Kwag, D.J. Lee, C.W. Park, Y.J. Kim, J. Power Sources 195 (2010) 6031–6036.
[42] H. Xiang, K. Zhang, G. Ji, J.Y. Lee, C. Zou, X. Chen, J. Wu, Carbon 49 (2011) 1787–1796.
[43] R. Yi, F. Dai, M.L. Gordin, S. Chen, D. Wang, Adv. Energy Mater. 3 (2013) 295–300.
[44] R. Yi, F. Dai, M.L. Gordin, H. Sohn, D. Wang, Adv. Energy Mater. 11 (2013) 1507–1515.
[45] H. Fukui, O. Hisashi, T. Hino, K. Kanamura, ACS Appl. Mater. Interfaces 4 (2010) 998–1008.
[46] H. Fukui, N. Nakata, K. Dokko, B. Takemura, H. Ohsuka, T. Hino, K. Kanamura, ACS Appl. Mater. Interfaces 3 (2011) 2318–2322.
[47] H. Fukui, H. Ohsuka, T. Hino, K. Kanamura, J. Power Sources 196 (2011) 371–378.
[48] H. Fukui, H. Ohsuka, T. Hino, K. Kanamura, J. Electrochem. Soc. 158 (2011) A550–A555.
[49] X. Liu, K. Xie, C.-M. Zheng, J. Wang, Z. Jing, J. Power Sources 214 (2012) 119–123.
[50] X. Liu, M.-C. Zheng, K. Xie, J. Liu, Electrochim. Acta 59 (2012) 304–309.
[51] P. Dibandjo, M. Graczyk-Zajac, R. Riedel, V.S. Pradeep, G.D. Soraru, J. Eur. Ceram. Soc. 32 (2012) 2495–2503.
[52] M. Graczyk-Zajac, L. Toma, C. Fasel, R. Riedel, Solid State Ionics 225 (2012) 522–526.
[53] J. Kaspar, M. Graczyk-Zajac, R. Riedel, Solid State Ionics 225 (2012) 527–531.
[54] R. Bhandavat, Z. Pei, G. Singh, Nanomater. Energy 1 (2012) 324–337.
[55] V.S. Pradeep, M. Graczyk-Zajac, M. Wilamowska, R. Riedel, G.D. Soraru, Solid State Ionics 262 (2014) 22–24, http://dx.doi.org/10.1016/j.ssi.2013.1008.1043.
[56] H. Fukui, K. Eguchi, H. Ohsuka, T. Hino, K. Kanamura, J. Power Sources 243 (2013) 152–158.
[57] H. Fukui, H. Ohsuka, T. Hino, K. Kanamura, J. Electrochem. Soc. 160 (2013) A1276–A1281.
[58] G. Liu, J. Kaspar, L.M. Reinold, M. Graczyk-Zajac, R. Riedel, Electrochim. Acta 106 (2013) 101–108.
[59] J. Kaspar, M. Graczyk-Zajac, R. Riedel, J. Power Sources 244 (2013) 450–455.
[60] Y.F. Gao, M. Graczyk-Zajac, R. Riedel, Electrochim. Acta 115 (2014) 665–670.
[61] P.D. Weidman, D. Ahn, R. Raj, J. Power Sources 249 (2014) 219–230.
[62] V.S. Pradeep, M. Graczyk-Zajac, R. Riedel, G.D. Soraru, Electrochim. Acta 119 (2014) 78–85.
[63] J. Kaspar, G. Mera, A.P. Nowak, M. Graczyk-Zajac, R. Riedel, Electrochim. Acta 56 (2010) 174–182.
[64] M. Graczyk-Zajac, C. Fasel, R. Riedel, J. Power Sources 196 (2011) 6412–6418.
[65] L.M. Reinold, M. Graczyk-Zajac, Y. Gao, G. Mera, R. Riedel, J. Power Sources 236 (2013) 224–229.
[66] S.-H. Baek, L.M. Reinold, M. Graczyk-Zajac, R. Riedel, F. Hammerath, B. Büchner, H.-J. Grafe, J. Power Sources 253 (2014) 342–348.
[67] G.M. Renlund, S. Prochazka, R.H. Doremus, J. Mater. Res. 6 (1991) 2716–2722.
[68] G.M. Renlund, S. Prochazka, R.H. Doremus, J. Mater. Res. 6 (1991) 2723–2734.
[69] G.D. Soraru, J. Sol–Gel Sci. Technol. 2 (1994) 843–848.
[70] C.G. Pantano, A.K. Singh, H. Zhang, J. Sol–Gel Sci. Technol. 14 (1999) 7–25.
[71] G.D. Soraru, S. Modena, E. Guadagnino, P. Colombo, J. Egan, C. Pantano, J. Am. Ceram. Soc. 85 (2002) 1529–1536.
[72] T. Momma, S. Aoki, H. Nara, T. Yokoshima, T. Osaka, Electrochem. Commun. 13 (2011) 969–972.
[73] H. Nara, T. Yokoshima, T. Momma, T. Osaka, Energy Environ. Sci. 5 (2012) 6500–6505.
[74] H. Nara, T. Yokoshima, M. Otaki, T. Momma, T. Osaka, Electrochim. Acta 110 (2013) 403–410.
[75] A.M. Wilson, J.N. Reimers, E.W. Fuller, J.R. Dahn, Solid State Ionics 74 (1994) 249–254.
[76] A.M. Wilson, W. Xing, G. Zank, B. Yates, J.R. Dahn, Solid State Ionics 100 (1997) 259–266.
[77] A.M. Wilson, G. Zank, K. Eguchi, W. Xing, J.R. Dahn, J. Power Sources 68 (1997) 195–200.
[78] A.M. Wilson, G. Zank, K. Eguchi, W. Xing, B. Yates, J.R. Dahn, Chem. Mater. 9 (1997) 1601–1606.
[79] W. Xing, A.M. Wilson, K. Eguchi, G. Zank, J.R. Dahn, J. Electrochem. Soc. 144 (1997) 2410–2416.
[80] W. Xing, A.M. Wilson, G. Zank, J.R. Dahn, Solid State Ionics 93 (1997) 239–244.

[81] J. Shen, D. Ahn, R. Raj, J. Power Sources 196 (2011) 2875–2878.
[82] R. Bhandavat, M. Cologna, G. Singh, Nanomater. Energy 1 (2012) 57–61.
[83] R. Bhandavat, G. Singh, J. Phys. Chem. C 117 (2013) 11899–11905.
[84] X. Liu, K. Xie, J. Wang, C. Zheng, Y. Pan, J. Mater. Chem. 22 (2012) 19621–19624.
[85] P. Kroll, J. Mater. Chem. 13 (2003) 1657–1668.
[86] P. Kroll, J. Non-Cryst. Solids 351 (2005) 1121–1126.
[87] P. Kroll, J. Mater. Chem. 20 (2010) 10528–10534.
[88] P. Kroll, MRS Proc. 1313 (2011).
[89] P. Colombo, G. Mera, R. Riedel, G.D. Soraru, J. Am. Ceram. Soc. 93 (2010) 1805–1837.
[90] Y.D. Blum, D.B. MacQueen, H.-J. Kleebe, J. Eur. Ceram. Soc. 25 (2005) 143–149.
[91] H.-J. Kleebe, G. Gregori, Y.D. Blum, F. Babonneau, Int. J. Mater. Res. 97 (2006) 699–709.
[92] G. Gregori, H.-J. Kleebe, Y.D. Blum, F. Babonneau, Int. J. Mater. Res. 97 (2006) 710–720.
[93] S.J. Widgeon, S. Sen, G. Mera, E. Ionescu, R. Riedel, A. Navrotsky, Chem. Mater. 22 (2010) 6221–6228.
[94] G. Mera, A. Navrotsky, S. Sen, H.-J. Kleebe, R. Riedel, J. Mater. Chem. A 1 (2013) 3826–3836.
[95] J. Cordelair, P. Greil, J. Eur. Ceram. Soc. 20 (2000) 1947–1957.
[96] H.-J. Kleebe, Y.D. Blum, J. Eur. Ceram. Soc. 28 (2008) 1037–1042.
[97] S. Martínez-Crespiera, E. Ionescu, H.-J. Kleebe, R. Riedel, J. Eur. Ceram. Soc. 31 (2011) 913–919.
[98] A. Saha, R. Raj, D.L. Williamson, J. Am. Chem. Soc. 89 (2006) 2188–2195.
[99] P.E. Sanchez-Jimenez, R. Raj, J. Am. Ceram. Soc. 93 (2010) 1127–1135.
[100] D. Ahn, R. Raj, J. Power Sources 195 (2010) 3900–3906.
[101] D. Ahn, R. Raj, J. Power Sources 196 (2011) 2179–2186.
[102] S.D. Beattie, D. Larcher, M. Morcrette, B. Simon, J.M. Tarascon, J. Electrochem. Soc. 155 (2008) A158–A163.
[103] G. Schierning, R. Theissmann, H. Wiggers, D. Sudfeld, A. Ebbers, D. Franke, V.T. Witusiewicz, M. Apel, J. Appl. Phys. 103 (2008) 084305.
[104] D. Larcher, C. Mudalige, A.E. George, V. Porter, M. Gharghouri, J.R. Dahn, Solid State Ionics 122 (1999) 71–83.
[105] M. Wilamowska, M. Graczyk-Zajac, R. Riedel, J. Power Sources 244 (2013) 80–86.
[106] J. Kaspar, C. Terzioglu, E. Ionescu, M. Graczyk-Zajac, S. Hapis, H.J. Kleebe, R. Riedel, Adv. Funct. Mater. (2014), http://dx.doi.org/10.1002/adfm.201303828 in press.
[107] O. Madelung, Semiconductors Data Handbook, Springer, Berlin, 2004.
[108] C. Haluschka, H.J. Kleebe, R. Franke, R. Riedel, J. Eur. Ceram. Soc. 20 (2000) 1355–1364.
[109] C. Haluschka, C. Engel, R. Riedel, J. Eur. Ceram. Soc. 20 (2000) 1365–1374.